J Therm Anal Calorim (2011) 105:251–257
DOI 10.1007/s10973-011-1375-2

Differential scanning calorimetry study of the solidification sequence of austenitic stainless steel

Darja Steiner Petrovič · Grega Klančnik · Miran Pirnat · Jožef Medved

Received: 23 November 2010 / Accepted: 24 January 2011 / Published online: 15 February 2011

Abstract The solidification sequence of austenitic stainless steels can be predicted with thermodynamic calculations. Another way is to use models where the value of the $Cr_{eq.}/Ni_{eq.}$ ratio determines the relationship between the solidification mode and the composition factor. In this study the solidification of AISI 304LN stainless steel at different cooling rates was studied using differential scanning calorimetry (DSC). The samples were linearly heated above the liquidus temperature to 1550 °C at heating rates of 5, 10, and 25 K/min. The solidification (cooling) scans from 1550 °C involved the same selected ramps. After the DSC measurements the samples were metallographically analyzed to reveal the variations in the solidification microstructures. The microhardness of the solidified samples was also measured. It was found that the cooling rate critically influenced the solidification. The solidification behavior, which depends on the cooling rate, determines the evolution of the microstructure. At the slowest cooling rates a relief-cell morphology was observed, and at the fastest cooling rate the formation of dendrites was evident. With an increasing cooling rate the liquidus temperature decreased and the reaction enthalpy increased.

Keywords DSC · Austenitic stainless steel · Solidification · Cooling rate

D. Steiner Petrovič (✉)
Institute of Metals and Technology, Lepi pot 11, 1000 Ljubljana, Slovenia
e-mail: darja.steiner@imt.si

G. Klančnik · J. Medved
Faculty of Natural Sciences and Engineering, University of Ljubljana, Aškerčeva 12, 1000 Ljubljana, Slovenia

M. Pirnat
Acroni d.o.o., Cesta Borisa Kidriča 44, 4270 Jesenice, Slovenia

Introduction

Stainless steels are considered as promising materials for many conventional and strategic applications in the power, chemical, petrochemical, refinery, pulp and paper, and marine sectors. Austenitic stainless steels have relatively modest mechanical properties, but these are largely outweighed by their excellent corrosion resistance in many media [1, 2]. Nitrogen-added austenitic stainless steels are a prospective material for reactor vessels and piping systems, primarily due to their good intergranular corrosion resistance along with desirable mechanical and fracture-mechanics properties. The use of such a material may provide a comparatively longer life with enhanced safety for any component requiring a higher resistance to rapid crack propagation, indicating a higher resistance to brittle fracture [3].

The structural evolution during the solidification of austenitic stainless steels plays a crucial role in the materials' properties [4]. The occurrence of the peritectic reaction is very important from the point of view of cracking. Peritectics are accompanied by volume shrinkages and elastic straining in the solidifying shell of the steel [5]. Hot cracking refers to the cracking that occurs during casting, hot working, or welding at temperatures close to the melting point of the material. This cracking can occur both above the liquation temperature (supersolidus cracking) and in the solid state (subsolidus cracking) [6].

Hot cracking has been investigated in castings and welds for several decades. The hot cracking in stainless steel is caused by low-melting eutectics containing impurities such as S, P and alloying elements such as Ti and Nb [6, 7].

The solidification mode of austenitic stainless steels has a large effect on the quality of the slabs, and consequently on the hot- and cold-rolled flat products [8]. The hot workability of the as-solidified microstructure is worse in

the case of the primary solidification to austenite, since, in this case, the amount of accumulated impurities in the final melt is greater. It has been reported that the much stronger effects of the impurities are due to their interphase segregation and the accumulation of inclusions [9, 10].

For austenitic stainless steels, the solidification mode involving $Cr_{eq.}/Ni_{eq.}$ is normally used to simplify a multi-component system into the Fe–Cr–Ni ternary system. It is divided into four types: austenitic (A), austenitic–ferritic or primary austenitic (AF), ferritic–austenitic or primary ferritic (FA), and ferritic (F). But, the proposed sets of expressions for Cr-equivalent and Ni-equivalent vary from one author to another [11]. In particular, in some of the Ni-equivalent formulae the effects of different chemical elements are valued differently. When using $Cr_{eq.}/Ni_{eq.}$, difficulties can arise in predicting the solidification mode, e.g., of the primary precipitated phase.

Solidification, from a thermal point of view, is a non-linear heat-conduction problem, expanded with a heat source corresponding to the released latent heat of solidification. This latent heat of solidification is one of the most important parameters for characterizing the solidification of cast iron [12].

The solidification sequence of austenitic stainless steels can also be predicted with thermodynamic calculations. Here, the equilibrium solidification conditions are assumed, whereas during solidification under industrial conditions, non-equilibrium conditions prevail. One of the aspects that plays an important role is the solidification rate, which is normally not uniform during the solidifying of the steel, e.g., in continuous casting or welding.

Thermal analysis is one of the methods appropriate for metallurgical process control and an investigation of the kinetics of solidification. The obtained cooling curves can be used for the interpretation of the solidification mechanisms [12]. Using thermal analysis, the magnitude of the undercooling during solidification can also be measured [13]. Differential scanning calorimetry (DSC) is a powerful technique that measures the enthalpy change of a sample under controlled conditions, e.g. in solidification or phase transformation studies [14, 15].

The aim of this study was to determine the effect of the cooling rate on the solidification and the microstructural evolution of the selected austenitic stainless steel AISI 304LN.

Materials and experimental procedures

The alloy used in this study was austenitic stainless steel AISI 304LN containing 0.1 mass% of nitrogen and 0.021 mass% of carbon.

The thermal analysis was performed using DSC in a STA-449 C Jupiter, Netzsch instrument. In dynamic measurements, the furnace was linearly heated above the liquidus temperature to 1550 °C at heating rates of 5, 10, and 25 K/min. The solidification (cooling) scans from 1550 °C involved the same selected cooling ramps. The DSC experiments were conducted under a static atmosphere of nitrogen of 99.999 vol.% purity to prevent both the de-nitrogenation of the steel and to minimize the surface oxidation. The empty corundum crucible was taken as a reference. The approximate sample dimensions were $3 \times 3 \times 3$ mm^3, with the sample weighing approximately 200 mg.

The thermodynamic calculations of the phase diagram were performed using TCW5.

For the metallographic examinations a Microphot FXA-Nikon light microscope equipped with a Hitachi HV-C20 AMP 3CCD video camera was used. The etching was performed using Murakami's and Beraha's etchants. The Vickers microhardness HV0.1 was measured using an Instron Wilson-Wolpert Tukon 2100B hardness tester in accordance with ISO 6507-1:2006.

Results and discussion

Thermodynamic calculations

The thermodynamic calculations were performed with TCW5 for the prediction of the solidification process of the steel. The chemical composition of the selected austenitic stainless steel AISI 304LN is given in Table 1.

Phase equilibria were calculated in the temperature range 500–2000 °C. In Fig. 1 mass-fraction of equilibrium phases in the selected temperature range is presented.

According to the equilibrium phase diagram presented in Fig. 1 the selected AISI 304LN steel solidifies with the primary formation of δ-ferrite, which has a b.c.c. crystallographic structure. The solidification proceeds in the three-phase region ($L + \delta + \gamma$) with the formation of the γ-phase, an austenite with the f.c.c. crystallographic structure. Under equilibrium cooling conditions δ-ferrite will transform into austenite and this phase will remain down to room temperature.

Table 1 Chemical composition of AISI 304LN/mass%

C	Cr	Ni	Mn	Cu	Si	N	Mo	Co	Nb	Ti
0.021	18.32	8.29	1.31	0.56	0.30	0.10	0.31	0.218	0.014	0.005

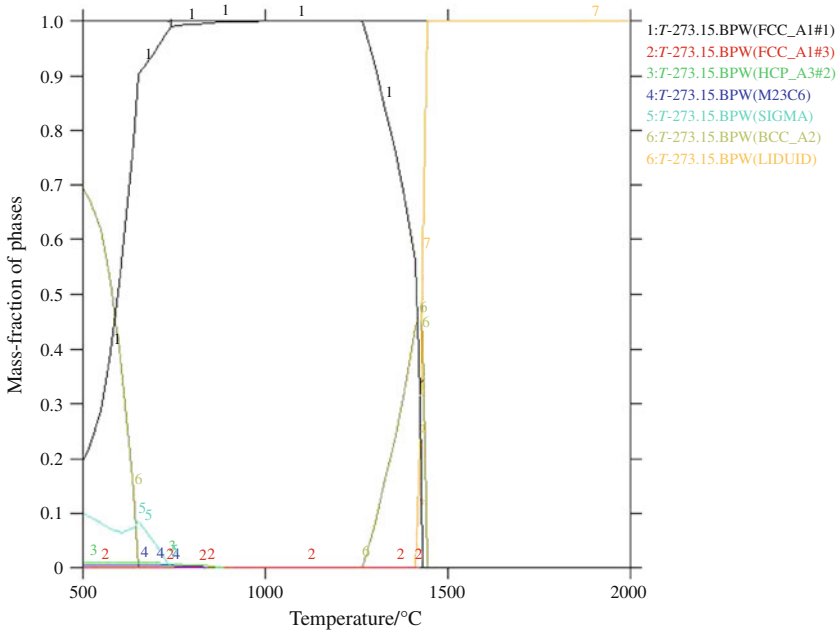

Fig. 1 Mass-fraction of equilibrium phases as a function of temperature for the AISI 304LN with the chemical composition given in Table 1

Solidification models based on the $Cr_{eq.}/Ni_{eq.}$ ratio

For austenitic stainless steels, the solidification mode using $Cr_{eq.}/Ni_{eq.}$ to simplify a multicomponent system into the Fe–Cr–Ni ternary system is normally used.

One of the models predicting the solidification mechanism using the $Cr_{eq.}/Ni_{eq.}$ ratio of austenitic stainless steels is presented in Table 2.

In Table 3 some of the proposed sets of expressions for the $Cr_{eq.}$ and $Ni_{eq.}$ are summarized.

From the calculated results given in Table 3 and the fact that there are many models available for predicting the solidification mechanism of austenitic stainless steels, it is evident that some difficulties can arise when predicting the solidification mode. It is evident that using different sets of formulae the results can be very scattered. Also, the presence of alloying elements other than Cr and Ni limit the use of available phase diagrams for assessing the solidification sequence [4]. Under non-equilibrium solidification conditions the segregations of elements alter the product of the evolved phases and their composition [6].

Differential scanning calorimetry

The aim of our investigation was to determine the effect of the cooling rate on the solidification of austenitic stainless steel using DSC. Steel samples were first linearly heated above the liquidus temperature at various heating rates (5, 10, and 25 K/min) to enable monitoring of their solidification behaviour.

The DSC melting spectra obtained were characterized by several endothermic peaks, whereas the DSC cooling spectra exhibited an exothermic peak. Typical examples of the obtained DSC heating/cooling curves of AISI 304LN are presented in Figs. 2 and 3.

The typical DSC melting spectrum obtained at a heating rate of 10 K/min is characterized by sequential melting, as confirmed by several endothermic peaks (Fig. 2). It is assumed that the endothermic peak involving 17.8 J/g of reaction enthalpy with a T_{onset} at about 798 °C represents the dissolving of precipitates (e.g., carbides, nitrides, and σ-phase) in the austenite. A minor exothermic peak was measured at around 1200 °C. The transformation of the retained δ-ferrite to γ is possible. The next endothermic

Table 2 Solidification mechanisms of austenitic stainless steels [4]

$(Cr_{eq.}/Ni_{eq.})$	Solidification mechanism	Mode
$(Cr_{eq.}/Ni_{eq.}) < 1.25$	$L \rightarrow L + \gamma_{prim.} \rightarrow \gamma$	A
$1.25 < (Cr_{eq.}/Ni_{eq.}) < 1.48$	$L \rightarrow L + \gamma_{prim.} \rightarrow L + \gamma + \delta \rightarrow \gamma + \delta$	AF
$1.48 < (Cr_{eq.}/Ni_{eq.}) < 1.95$	$L \rightarrow L + \delta_{prim.} \rightarrow L + \delta + \gamma \rightarrow \gamma + \delta$	FA
$(Cr_{eq.}/Ni_{eq.}) < 1.95$	$L \rightarrow L + \delta_{prim.} \rightarrow \delta \rightarrow \gamma + \delta$	F

L liquid, γ austenite, δ delta ferrite, *A* austenitic, *AF* austenitic–ferritic, *FA* ferritic–austenitic, *F* ferritic

Table 3 Set of formulae for calculating $Cr_{eq.}$ and $Ni_{eq.}$ [4, 11, 16–18]

	Set of formulae	Author/Year	Calculated ($Cr_{eq.}$/$Ni_{eq.}$) of AISI 304LN
1	$Cr_{eq.} = Cr + Mo + 1.5\ Si + 0.5\ Nb$ $Ni_{eq.} = Ni + 0.5\ Mn + 30\ C$	Schaeffler/1949	1.99
2	$Cr_{eq.} = Cr + Mo + 1.5\ Si + 0.5\ Nb$ $Ni_{eq.} = Ni + 0.5\ Mn + 30\ C + 12\ N$	Rajasekhar/1997	1.77
3	$Cr_{eq.} = Cr + 1.37\ Mo + 1.5 \bullet Si + 2\ Nb + 3\ Ti$ $Ni_{eq.} = Ni + 0.31\ Mn + 22\ C + 14.2\ N + Cu$	Hammar, Svensson/1979	1.72
4	$Cr_{eq.} = Cr + Mo + 1.5\ Si$ $Ni_{eq.} = Ni + 0.5\ Mn + 30\ C + 18\ N$	Koseki/1995	1.67
5	$Cr_{eq.} = Cr + Mo + 0.7\ Nb$ $Ni_{eq.} = Ni + 35\ C + 20\ N + 0.25\ Cu$	Siewert/1988	1.66
6	$Cr_{eq.} = Cr + Mo + 1.5\ Si + 0.5\ Nb$ $Ni_{eq.} = Ni + 0.5\ Mn + 30\ C + 30\ N$	DeLong/1956	1.51
7	$Cr_{eq.} = Cr + Mo + 1.5\ Si + 0.5\ Nb + 2\ Ti$ $Ni_{eq.} = Ni + 0.5\ Mn + 30\ C + 30\ N + 0.5\ Cu + 0.5\ Co$	[18]	1.47

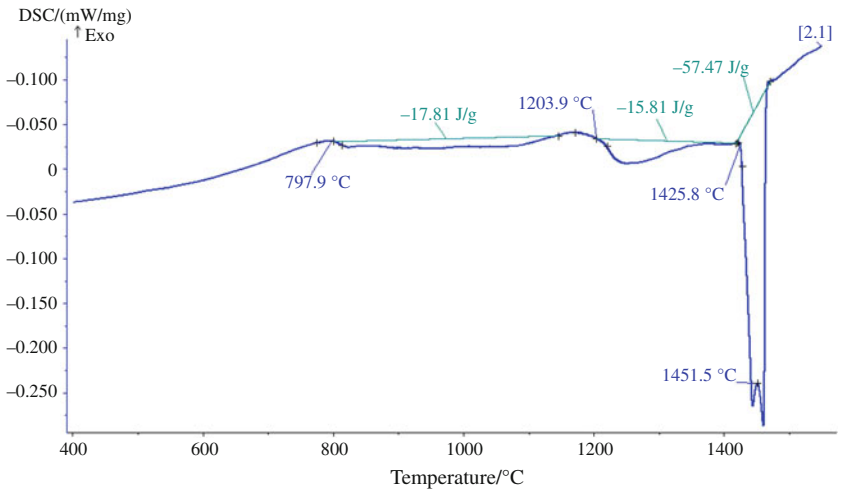

Fig. 2 Melting curve of the AISI 304LN (static nitrogen atmosphere; heating rate 10 K/min)

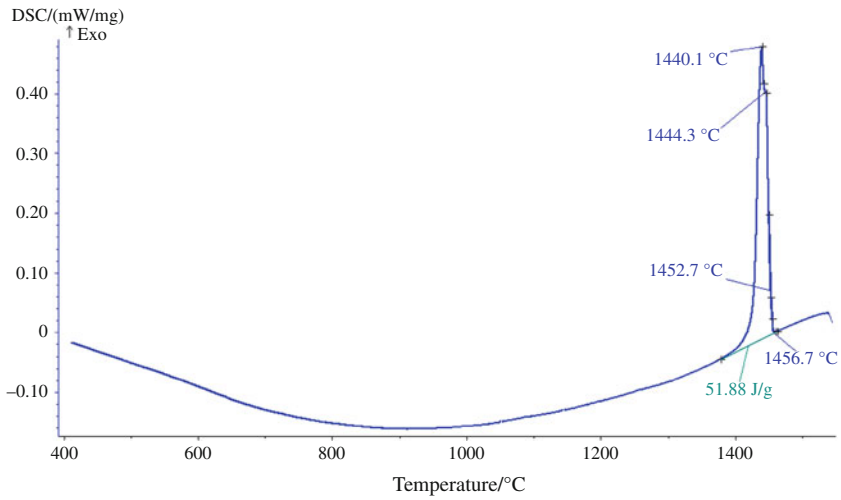

Fig. 3 Cooling curve of the AISI 304LN (static nitrogen atmosphere; cooling rate 10 K/min)

peak involving 15.8 J/g of enthalpy can be ascribed to the $\gamma \rightarrow \delta$ transformation. The T_{onset} of the major endothermic reaction(s) is around 1426 °C (solidus temperature). The solidus temperature quantifies the point at which a material is completely solidified. Above the solidus temperature the melting two phases proceeds. First, the melting of austenite and then the melting of δ-ferrite (see Fig. 1). The two endothermic reactions evolved 57.47 J/g of enthalpy.

A typical DSC cooling curve is presented in Fig. 3, where the T_{onset} of the major exothermic reaction(s) corresponds to solidification.

DSC solidification curves can be used for interpreting the solidification mechanisms, so we have compared the exothermic peaks evolved during cooling. The details are shown in Fig. 4. The liquidus temperatures were not identical for the three scan rates, demonstrating that the cooling rate has a significant effect on the solidification reactions due to non-equilibrium conditions. The lowest liquidus temperature was measured at the fastest cooling rate (1442.9 °C) and, vice versa, the highest liquidus temperature was measured at slower cooling rates (1454.7 and 1456.7 °C).

During solidification at the slowest cooling rate (5 K/min) two exothermic peaks were observed. The reaction sequence of the solidification was confirmed with two other cooling rates, i.e., 10 and 25 K/min. This event in the thermal behavior during solidification was even more pronounced at the fastest cooling rate (Fig. 4).

The assumed peritectic reaction was determined only at a cooling rate of 10 K/min, at a temperature of 1452.7 °C. However, peritectic reactions are difficult to determine, especially if this reaction starts close to the liquidus temperature (5 and 10 K/min).

The value of reaction enthalpy in the solidification interval increased with an increasing cooling rate.

The width of the solidification interval increased with the increasing cooling rate. The interval of solidification is determined from the liquidus temperature to the peak maximum in the last solidification stage. At 5, 10, and 25 K/min the values of solidification interval correspond to 7.2, 16.6, 27.2 °C, respectively. The peak's maximum in the last solidification rate corresponds to the temperature where most of the liquid phase has solidified. The peak's maximum (1448.7, 1440.1 °C and 1415.7 for 5, 10, and 25 K/min) also indicates that the remaining liquid (with Ni-enriched) after primary solidification solidifies at lower temperatures with faster cooling rates. From the peak's slope it can be assumed that the segregation of Ni increases with the increasing cooling rate due to non-equilibrium conditions.

Metallographic analyses

After the DSC experiments the effect of the cooling rate on the solidification microstructures of the austenitic stainless steel was examined metallographically.

Figure 5 shows a representative micrograph of the microstructure of the received industrial sample of AISI 304LN. The steel solidified under non-equilibrium conditions. The microstructure consists of austenite with some retained δ-ferrite.

Figures 6, 7, and 8 show the morphologies of the as-solidified structures after the controlled solidification. The controlled solidification with continuous cooling was conducted at cooling rates of 5, 10, and 25 K/min.

The relief-cell morphology was evident after the solidification during cooling at 5 and 10 K/min. In the sample that solidified at a cooling rate of 10 K/min the microstructure was composed of light- and dark-colored phases, assumingly austenite and δ-ferrite (Fig. 7).

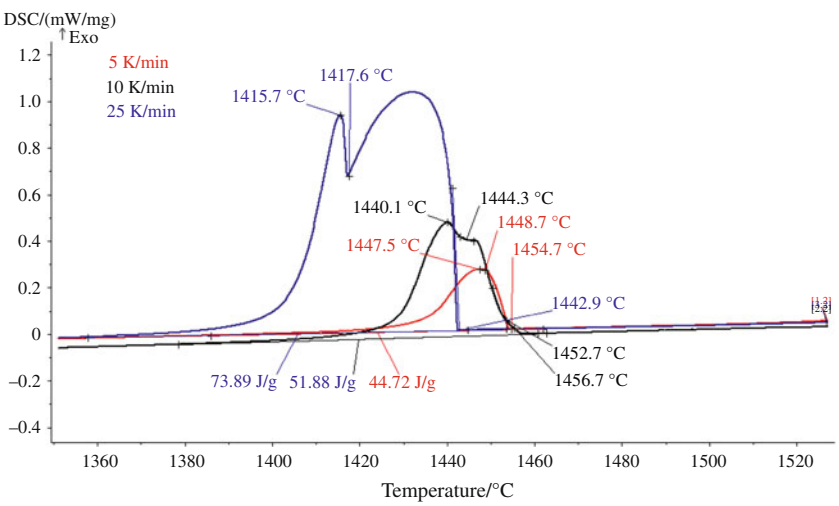

Fig. 4 Details of the DSC solidification curves for AISI 304LN obtained at various cooling rates (5, 10, and 25 K/min)

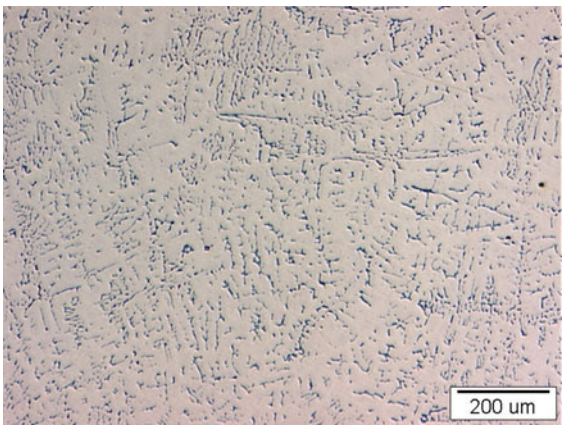

Fig. 5 As-received structure of AISI 304LN (LM: ×50; Etchant: Murakami's)

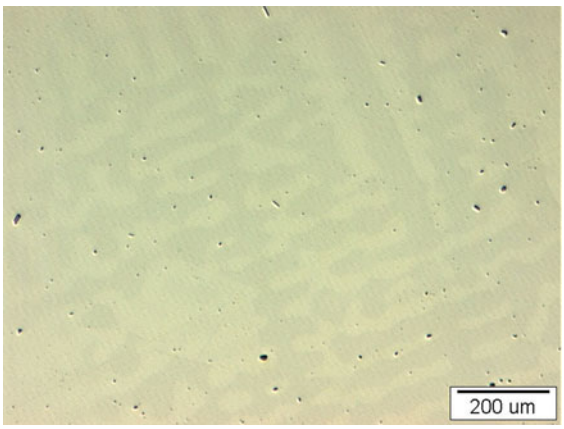

Fig. 8 As-solidified structure of AISI 304LN (cooled at 25 K/min; LM: ×50, Etchant: Beraha's)

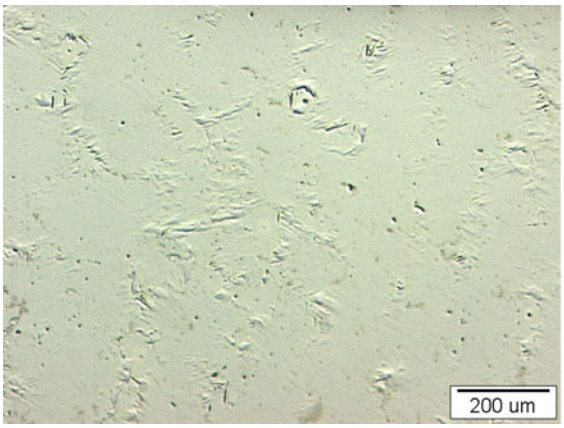

Fig. 6 As-solidified structure of AISI 304LN (cooled at 5 K/min; LM: ×50, Etchant: Beraha's)

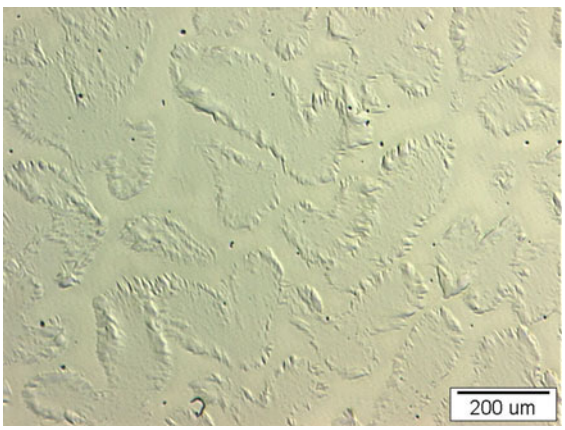

Fig. 7 As-solidified structure of AISI 304LN (cooled at 10 K/min; LM: ×50, Etchant: Beraha's)

After the solidification with the fastest cooling rate (25 K/min) the as-solidified structure exhibits the formation of dendrites. The residual liquid that was the last to solidify appeared as a light-colored phase between the precipitated dendrites (Fig. 8). This is in good agreement with the DSC cooling curves, which exhibit the most intensive undercooling obtained during cooling at that rate (25 K/min).

δ-Ferrite is the primary phase formed in the solidification process of the selected AISI 304LN, as confirmed by thermodynamic and the metallographic analysis.

The constitutional undercooling is reached during solidification when the solute elements segregate in front of the growth interface of the δ-ferrite and the liquidus temperature decreases with the increment of the solute content. The rejection of the solute at the solidifying interface can lead to enrichments of the interdendritic areas with respect to the austenite-stabilizing elements [19].

Table 4 lists the results of the microhardness measurements for the as-solidified microstructures.

The average hardness of the mostly uniform morphology of the microstructure solidified at 5 K/min was 370 HV. In the microstructure of the sample solidified at 10 K/min the hardness of the light-colored phase was 205 HV, and that of the dark-colored phase was 383 HV. A separate hardness measurement of the two phases visible in Fig. 8 was not possible due to the limitations of the testing method. The average hardness of the sample solidified at 25 K/min was 185 HV.

The results of the microhardness measurements suggest that the dark-colored phase is primarily solidified δ-ferrite. Based on these measurements it is assumed that the volume fraction of austenite increases with an increasing cooling rate.

Table 4 Vickers microhardness HV0.1 of the as-solidified microstructures

Sample (cooling rate)	HV0.1		
	Average	Light-colored phase	Dark-colored phase
AISI304LN (5 K/min)	370	–	–
AISI304LN (10 K/min)	–	205	383
AISI304LN (25 K/min)	185	–	–

Conclusions

DSC curves of the austenitic stainless steel AISI 304LN clearly show the influence of the various cooling rates on the solidification sequence.

The cooling rate has an influence on the liquidus temperature and the width of the solidification interval. The liquidus temperature decreases with an increasing cooling rate. The value of reaction enthalpy in the solidification interval increases with an increasing cooling rate.

The δ-ferrite is the primary phase formed in the solidification process of the selected AISI 304LN, as confirmed by thermodynamic and the metallographic analyses. The use of the $Cr_{eq.}/Ni_{eq.}$ ratio for assessing the solidification sequence of austenitic stainless steel is limited.

It was found that the solidification behavior, depending on the cooling rate, determines the microstructure evolution. The relief-cell morphology was evident after the solidification at the slowest cooling rates. After the solidification with the fastest cooling rate the as-solidified structure exhibits the formation of dendrites.

Acknowledgements The authors would like to acknowledge Acroni d.o.o., Jesenice, Slovenia, for its financial support of this study and the supply of the steel. The authors also gratefully acknowledge Mrs. N. Lipovšek, from IMT for her technical assistance. The work was also supported by the Slovenian Research Agency (Pr.No. P2-0050).

References

1. Bhadeshia HKDH, Honeycombe RWK. Steels. 3rd ed. Amsterdam: Elsevier; 2007. p. 270.
2. Torkar M, Mandrino Dj, Lamut M. An AES investigation of brushed AISI 304 stainless steel after corrosion testing. Materiali in tehnologije. 2008;42:39–43.
3. Kulkarni S, McCowan CN, Olson DL. Improvement of weld characteristics by variation in welding processes and parameters in joining of thick wall 304LN stainless steel pipe. ISIJ Int. 2008;48:1560–9.
4. Rajasekhar K, Harendranath CS, Raman R, Kulkarni SD. Microstructural evolution during solidification of austenitic stainless steel weld metals: a color metallographic and electron microprobe analysis study. Mater Charact. 1997;38:53–65.
5. Nassar H, Korojy B, Fredriksson H. A study of shell growth irregularities in continuously cast 310S stainless steel. Ironmaking Steelmaking. 2009;36:521–8.
6. Shankar V, Gill TPS, Mannan SL, Sundaresan S. Solidification cracking in austenitic stainless steel welds. In: Raj B, Rao KBS, editors. Frontiers in materials science. Bangalore: Universities Press; 2005. p. 359–82.
7. Lee DJ, Byun JC, Sung JH, Lee HW. The dependence of crack properties on thr *Cr/Ni* equivalent ratio in AISI 304L austenitic stainless steel weld metals. Mater Sci Eng A. 2009;513–4:154–9.
8. Huang FX, Wang XH, Zhang JM, et al. In situ observation of solidification process of AISI 304 austenitic stainless steel. J Iron Steel Res Int. 2008;6:78–82.
9. Tehovnik F, Arzenšek B, Arh B. Tensile tests on stainless steels in temperature range 800 to 1200 °C. Metalurgija. 2008;47:75–9.
10. Tehovnik F, Vodopivec F, Arzenšek B, Celin R. The effect of lead on the hot workability of austenitic stainless steel with a solidification structure. Metalurgija. 2010;49:49–52.
11. Davis JR. Stainless steels. Materials Park: ASM International; 1999. p. 370.
12. Dioszegi A, Svensson IL. On the problems of thermal analysis of solidification. Mater Sci Eng A. 2005;413–4:474–9.
13. Naglič I, Smolej A, Doberšek M, Mrvar P. The influence of TiB_2 particles on the effectiveness of Al-3Ti-0.15C grain refiner. Mater Charact. 2008;59:1458–65.
14. Arockiasamy A, German RM, Wang P, Horstemeyer MF, Suri P, Park SJ. DSC analysis of Al6061 aluminium alloy powder by rapid solidification. J Therm Anal Calorim. 2010;100:361–6.
15. Gazda A. Analysis of decomposition processes of ausferrite in copper-nickel austempered ductile iron. J Therm Anal Calorim. 2010;102:923–30.
16. Schaeffler AL. Constitution diagram for stainless steel weld metal. Met Prog. 1949;56:680.
17. Koseki T, Inoue H, Morimoto H, Ohkita S. Prediction of solidification and phase transformation of stainless steel weld metals. Nippon Steel Tech Rep. 1995;65:33–40.
18. Pohar C, Klinar M, Kosmač A. Correlation of the occurrence of surface cracks on stainless-steel heavy plates with ferrite numbers and crack indexes. Materiali in tehnologije. 2004;38:185–90.
19. Liang GF, Wan CQ, Wu JC, Zhu GM, Yu Y, Fang Y. In-situ observation of growth behaviour and morphology of delta-ferrite as function of solidification rate in an AISI304 stainless steel. Acta Metall Sin. 2006;19:441–8.